MxiN Differentially Regulates Monomeric and Oligomeric Species of the *Shigella* Type Three Secretion System ATPase Spa47

Heather B. Case[1] and Nicholas E. Dickenson[1*]

[1]Department of Chemistry and Biochemistry, Utah State University, Logan, UT 84322

***To whom correspondence should be addressed:** Department of Chemistry and Biochemistry, Utah State University, Logan, UT 84322, 0300 Old Main Hill, Logan, UT 84321, Tel. 435-797-0982, Email: nick.dickenson@usu.edu

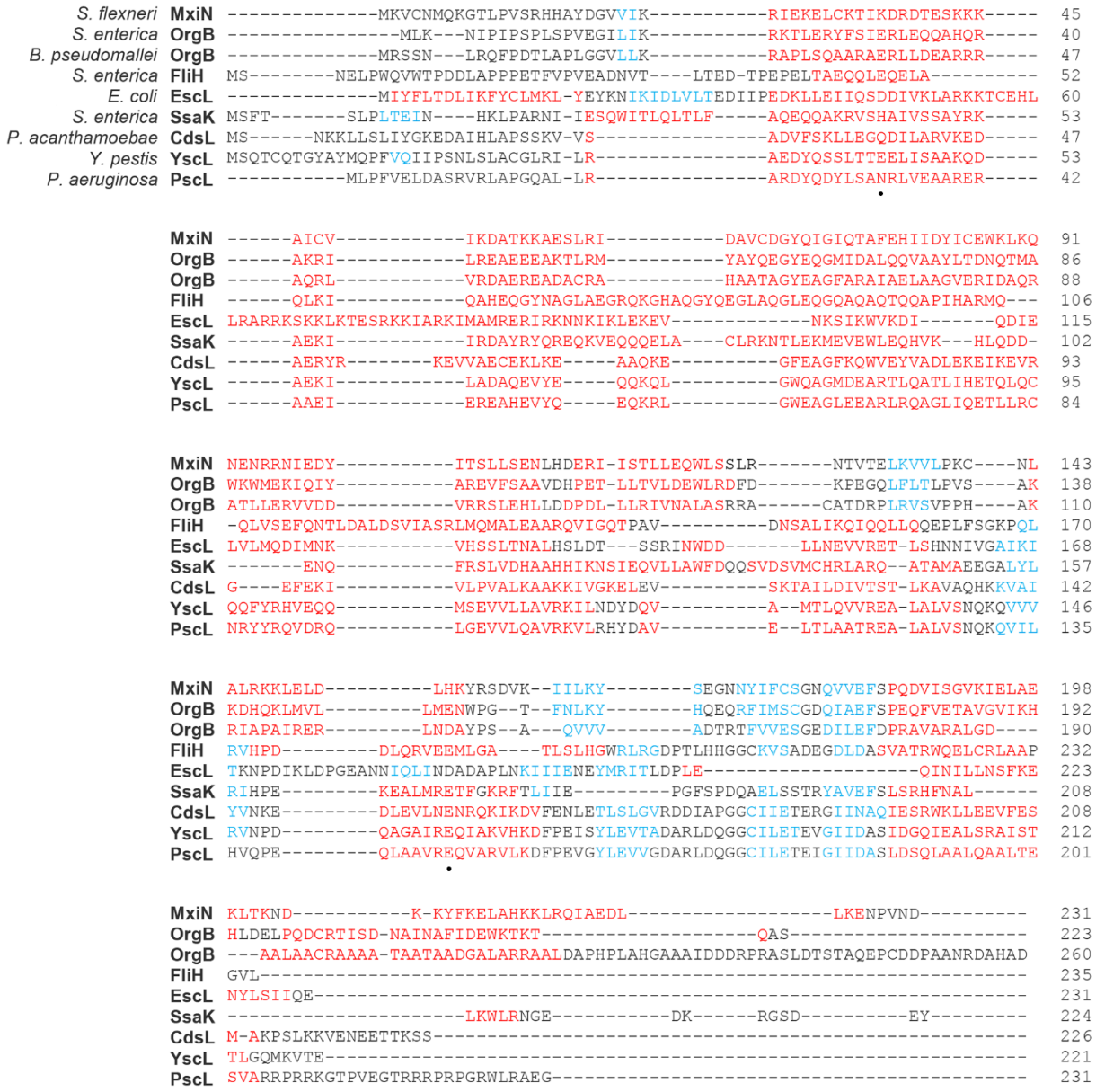

Supplementary Figure S1. Multiple sequence alignment of MxiN and putative MxiN homologs. Protein sequence alignment of MxiN (T3SS, *S. flexneri*), OrgB (T3SS, *S. enterica*), OrgB (T3SS, *B. pseudomallei*), FliH (Flagellum, *S. enterica*), EscL (T3SS, *E. coli*), SsaK (T3SS, *S. enterica*), CdsL (T3SS, *P. acanthamoebae*), YscL (T3SS, *Y. pestis*), and PscL (T3SS, *P. aeruginosa*) was performed using the UniProt multiple sequence alignment tool, Clustal Omega, with single fully conserved residues (*), conservation between groups with strongly similar properties (:), and weakly similar properties (.) identified. α-helical and β-sheet regions, as predicted by the PSIPRED structure prediction server, are color-coded red and blue, respectively. UniProt accession numbers used for sequence alignment are Q6XVX6, B8Y8F4, A0A0H5JKW6, P15934, Q9AJ30, A0A0F7J8U0, F8KV23, P69976, P95440 for MxiN, OrgB (*Salmonella*), OrgB (*Burkholderia*), FliH, EscL, SsaK, CdsL, YscL, and PscL, respectively.

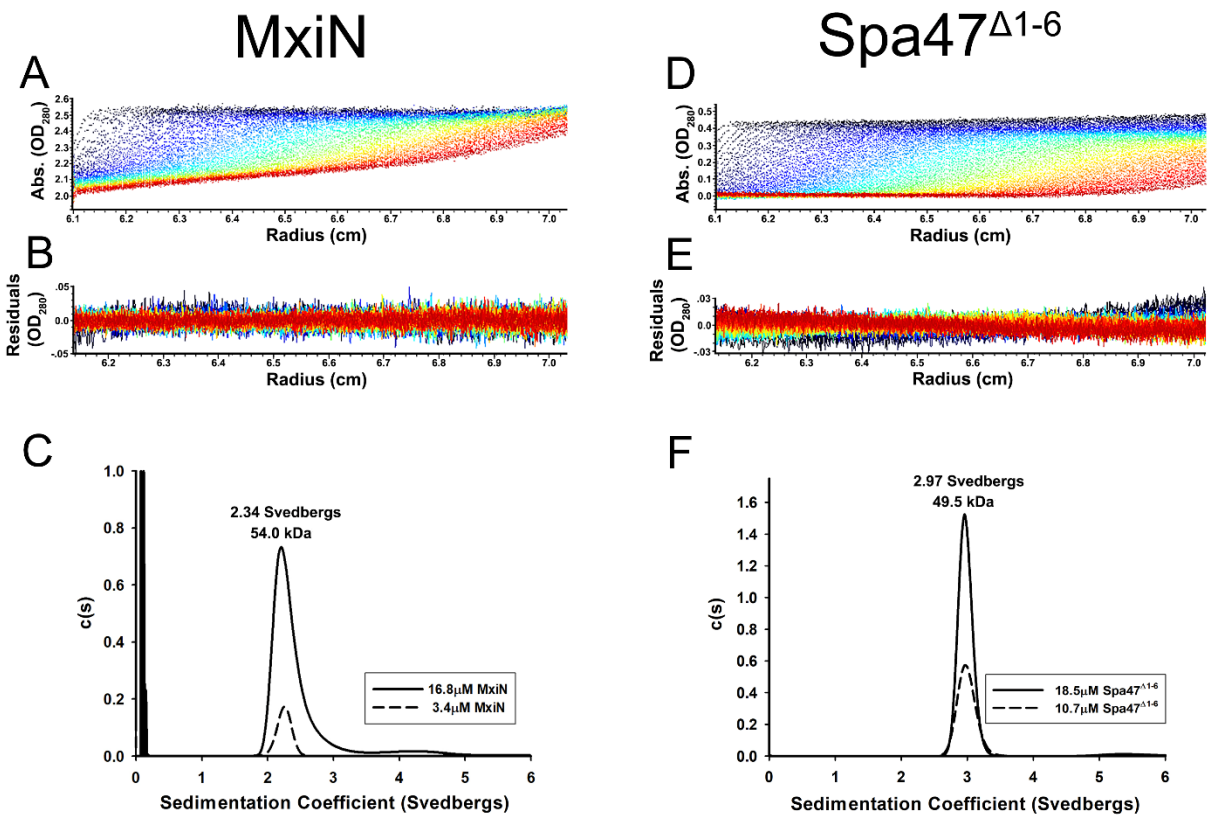

Supplementary Figure S2. AUC analysis of MxiN and Spa47$^{\Delta 1\text{-}6}$. A_{280} absorbance scans of **A)** MxiN and **D)** Spa47$^{\Delta 1\text{-}6}$ monitored during SV-AUC. Representative residuals from fitting the **B)** MxiN and **E)** Spa47$^{\Delta 1\text{-}6}$ data to a continuous c(s) distribution model. Sedimentation coefficient distributions (c(s) versus S) for **C)** MxiN and **F)** Spa47$^{\Delta 1\text{-}6}$. MxiN sediments as primarily a single species with a sedimentation coefficient of 2.87 Svedbergs and a calculated molecular mass of 54.0 kDa, consistent with a MxiN homo-dimer. Spa47$^{\Delta 1\text{-}6}$ sediments as a single dominant species with a sedimentation coefficient of 2.97 Svedbergs and a calculated molecular mass of 49.5 KDa, corresponding to monomeric Spa47$^{\Delta 1\text{-}6}$. A minor peak in the Spa47$^{\Delta 1\text{-}6}$ distribution is also seen at 5.5 Svedbergs, consistent with the previously characterized Spa47 homo-trimer. Each protein was analyzed at two concentrations to ensure the sedimentation results are concentration-independent.

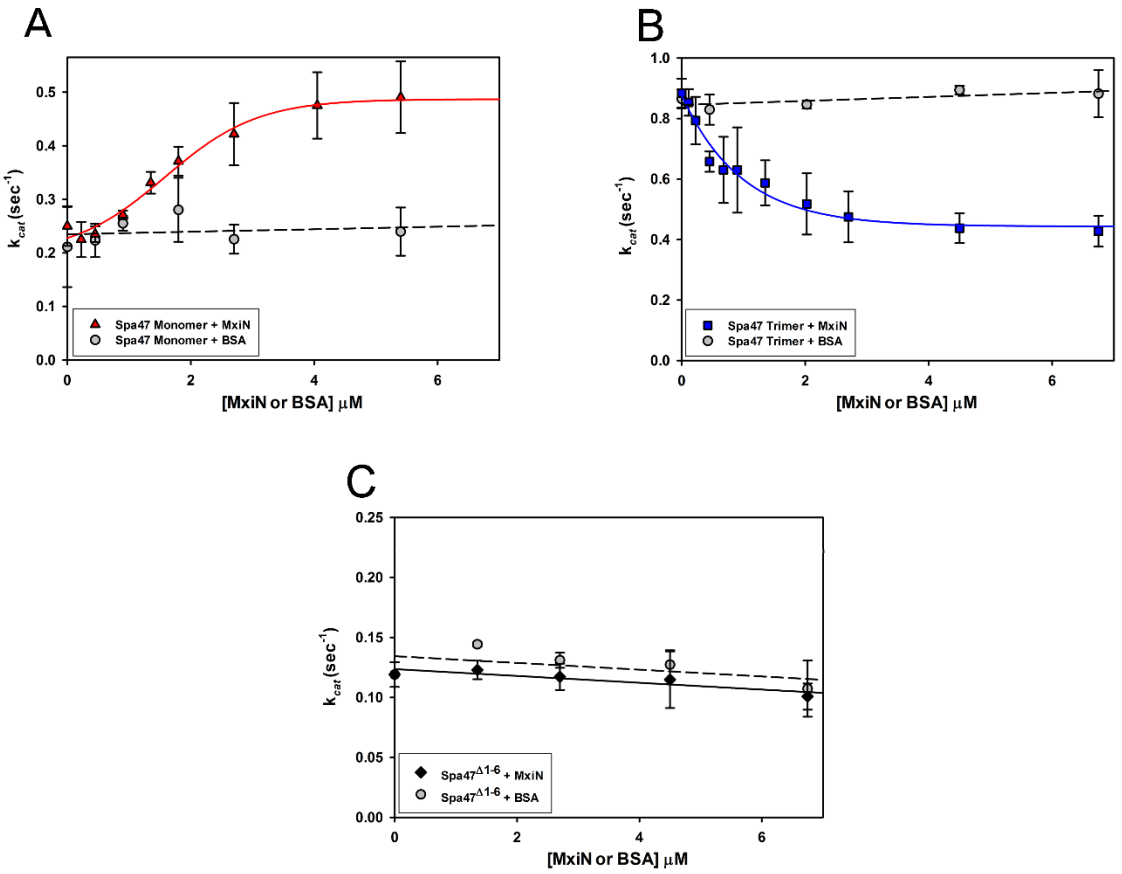

Supplementary Figure S3. Individual Spa47 activity profiles as a function of MxiN concentration. The effect of MxiN on the activity of **A)** Spa47 monomer, **B)** Spa47 trimer, and **C)** $Spa47^{\Delta 1-6}$ was tested as described for Figure 6A in the main text. Bovine serum albumin was additionally substituted for MxiN and plotted as a control to ensure that the observed effects of MxiN on Spa47 are not due to molecular crowding or non-specific protein interactions. The addition of BSA did not significantly affect the rate of ATP hydrolysis of any of the tested Spa47 constructs, ensuring that the effects seen by MxiN are specific.

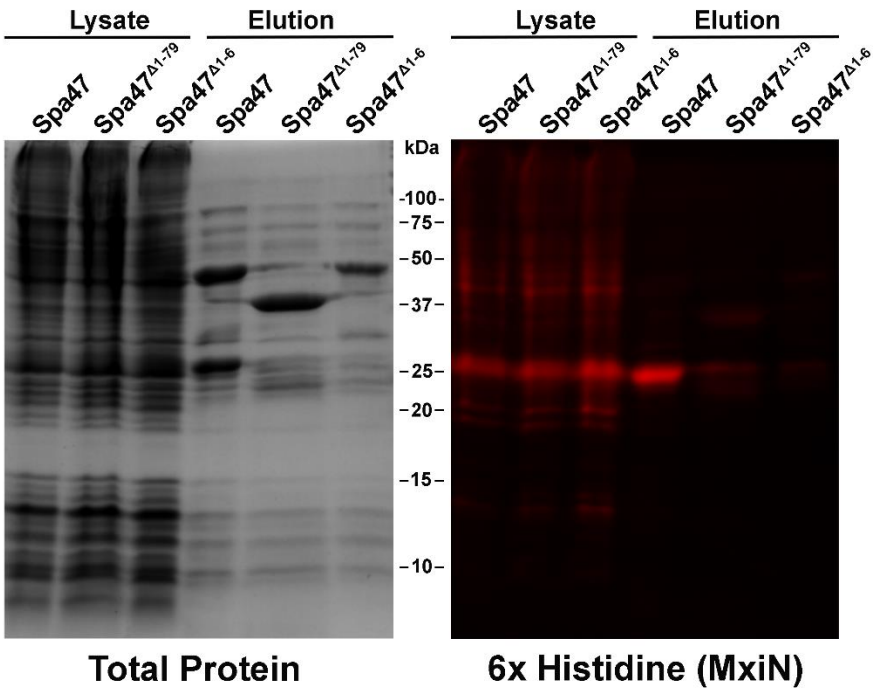

Supplementary Figure S4. The N-terminus of Spa47 supports MxiN/Spa47 complex formation. MxiN was cloned into pET15b, providing an N-terminal 6X-Histidine tag and each of the tested Spa47 constructs were cloned into pTYB21 to allow purification via an N-terminal chitin binding domain. MxiN was co-expressed in *E. coli* with Spa47, Spa47$^{\Delta 1\text{-}79}$, or Spa47$^{\Delta 1\text{-}6}$. Soluble cell lysates of the co-expressions were exposed to chitin resin to bind the N-terminal chitin binding domain on the Spa47 constructs and additionally retain any MxiN that was interacting directly with the Spa47. On column cleavage of the intein linker located between the chitin binding domain and Spa47 protein released Spa47 and any Spa47-bound MxiN from the column. Soluble cell lysates and the elution fractions of each MxiN/Spa47 co-expression were separated by SDS-PAGE and analyzed by total protein staining (left image) and a western blot probing for MxiN using monoclonal mouse anti-histidine primary antibodies and fluorescent Alexa 647 goat anti-mouse secondary antibodies (right image). MxiN is visible in all cell lysates at approximately 25 KDa in both the total protein stain and western blot, showing that it was properly expressed. As expected, full-length Spa47, Spa47$^{\Delta 1\text{-}79}$, and Spa47$^{\Delta 1\text{-}6}$ are all visible in the appropriate elution fractions of the total protein stained gel. MxiN efficiently co-purified with full-length Spa47 while little-to-no MxiN was detected in the Spa47$^{\Delta 1\text{-}79}$, and Spa47$^{\Delta 1\text{-}6}$ co-expressions, identifying the Spa47 N-terminus as critical for proper MxiN/Spa47 complex formation.

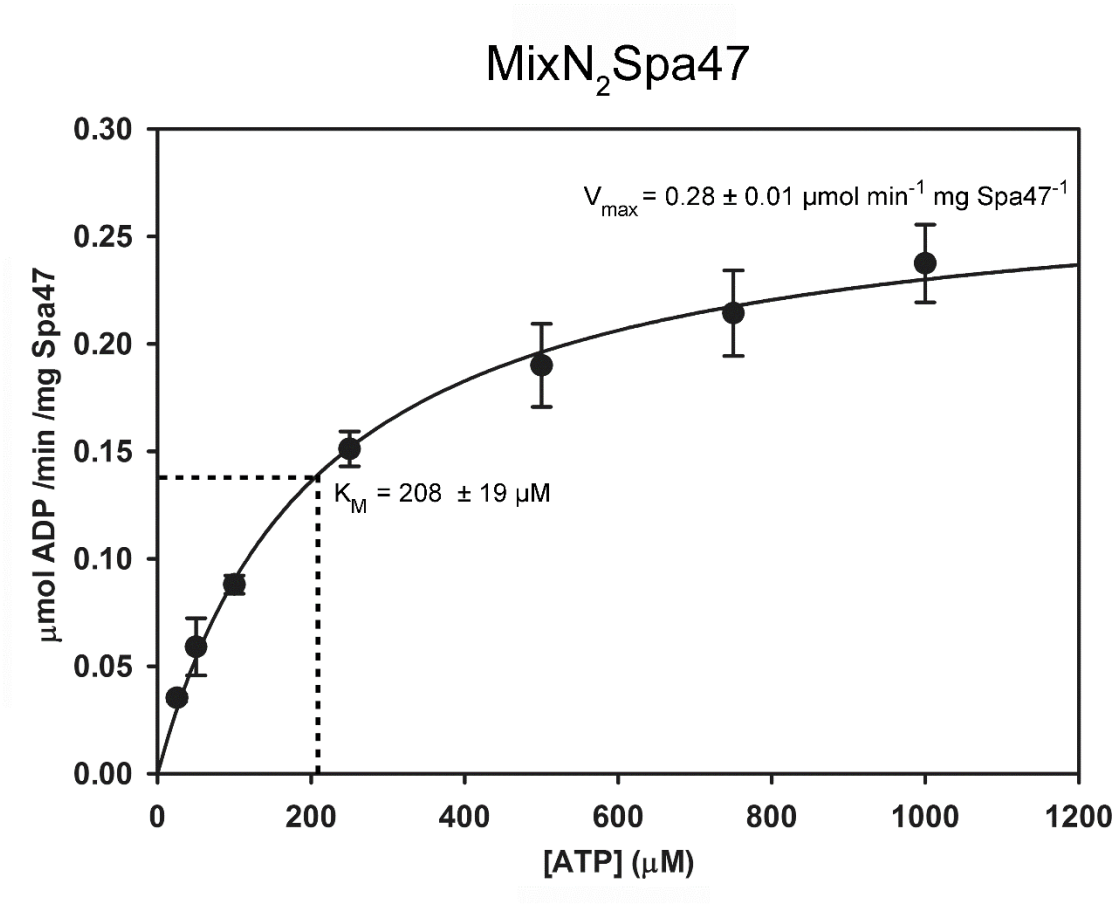

Supplementary Figure S5. Substrate-dependent ATPase activity profile for co-expressed and co-purified MxiN$_2$Spa47. MxiN and Spa47 were co-expressed and co-purified, identifying a stable MxiN$_2$Spa47 heterotrimer (**Figure 6**). The ATPase activity of the MxiN$_2$Spa47 complex was tested as a function of substrate concentration using the same α-^{32}P-ATP hydrolysis assay method described in the paper and a final MxiN$_2$Spa47 concentration of 0.16 µM. The initial velocity of each the reaction was plotted as a function of ATP concentration and fit to the Michaelis-Menten equation to determine the kinetic parameters K_M and V_{max}. The data are plotted as the average ± standard deviation resulting from triplicate analyses.